Scientia Iranica C (2019) 26(3), 1447–1456

Sharif University of Technology
Scientia Iranica
Transactions C: Chemistry and Chemical Engineering
http://scientiairanica.sharif.edu

Synthesis and characterization of poly(styrene-*block*-acrylic acid)/Fe_3O_4 magnetic nanocomposite using reversible addition-fragmentation chain transfer polymerization

M. Abbasian[a,*], L. Razavi[a], M. Jaymand[b], and S. Ghasemi Karaj-Abad[a]

a. *Department of Chemistry, Payame Noor University, Tehran, P.O. Box 19395-3697, Iran.*
b. *Immunology Research Center, Tabriz University of Medical Sciences, Tabriz, Iran.*

Received 15 November 2016; received in revised form 7 August 2018; accepted 12 January 2019

KEYWORDS
Poly(styrene-*block*-acrylic acid); RAFT polymerization; Fe_3O_4 nanoparticles; Nanocomposite .

Abstract. A well-defined amphiphilic poly(styrene-*block*-acrylic acid) (PSt-*b*-PAA) block copolymer to prepare a magnetic nanocomposite was synthesized by reversible addition-fragmentation chain transfer (RAFT) polymerization. The synthesized PSt and PSt-*b*-PAA copolymer was characterized using FTIR and ^{1}H NMR spectroscopies as well as GPC analysis. Afterwards, a PSt-*b*-PAA/Fe_3O_4 magnetic nanocomposite was fabricated through the incorporation of Fe_3O_4 nanoparticles (NPs) into the synthesized block copolymer. The morphology of the fabricated magnetic nanocomposite was observed using SEM and TEM. The SEM image revealed that the PSt-*b*-PAA/Fe_3O_4 magnetic nanocomposite had spherical morphology with the mean diameter of 100 nm, approximately. In addition, thermal properties of the synthesized polymers as well as the magnetic nanocomposite were studied using DSC and TGA analyses. The developed nanocomposite may be applied for enzyme immobilization and cell separation.

1. Introduction

Magnetic nanocomposites are a class of functional materials that have potential use in a broad variety of applications such as cell separation, enzyme immunoassay, and drug delivery due to their unique physicochemical properties including super-paramagnetism, high saturation magnetization, and high magnetic susceptibility [1-4]. Polymer/Fe_3O_4 magnetic nanocomposites are a kind of polymeric magnetic nanocomposites with magnetism obtained *via* a certain method for combining organic polymer and inorganic magnetic nanoparticles [5-9]. This type of magnetic nanocomposites has received a great deal of interest mainly due to its various applications, including magnetic separation, which is a relatively rapid and facile approach in comparison with other separation strategies [10-16].

Poly(styrene-*block*-acrylic acid) (PSt-*b*-PAA) amphiphilic copolymers have been investigated as an important copolymer model for the study of self-assembling and drug delivery systems [17-21]. PAA is a biocompatible material and has widely been applied as a pH-responsive drug carrier due to the carboxylic groups accepting protons at low pH values and releasing protons at high pH values [22]. In addition, hydrophobic PSt core remains glassy up to

*. *Corresponding author. Tel.: +98 41 35492301; Fax: +98 41 35492301*
E-mail addresses: m_abbasian@pnu.ac.ir and m_abbasian20@yahoo.com (M. Abbasian); m_jaymand@yahoo.com and m.jaymand@gmail.com (M. Jaymand)

doi: 10.24200/sci.2019.21232

the boiling point of water, which enhances the stability of micelles and has potential application in solubilizing hydrophobic substances [23]. PSt-*b*-PAA amphiphilic copolymers have been reported to be prepared by atom transfer radical polymerization (ATRP) [24-26] and Nitroxide-Mediated Polymerization (NMP) [27].

Living free radical polymerization has been introduced for the synthesis of macromolecules with predetermined molecular weights and narrow dispersity. Great progress has been made in controlled/living free radical polymerization in the past few decades toward the synthesis of complex and well-defined macromolecular architectures [28-38]. However, until now, these techniques have seldom been used in the synthesis of PSt-*b*-PAA by RAFT polymerization method. The most important advantage of RAFT process, in comparison with ATRP technique, is no metal contamination in the final polymer, which approves this approach for the synthesis of polymeric materials for biomedical purposes. In the case of NMP technique, the condition of reaction is hard and serious and very limited monomers can be polymerized by this method [33].

In this work, a facile method for preparing a PSt-*b*-PAA/Fe_3O_4 magnetic nanocomposite *via* a combination of RAFT polymerization and solution methods will be discussed. First, amphiphilic PSt-*b*-PAA copolymer was synthesized using RAFT polymerization technique. Afterwards, Fe_3O_4 NPs were synthesized through a co-precipitation approach and then, incorporated into the synthesized PSt-*b*-PAA copolymer via a solution mixing method.

2. Experimental

2.1. Material

The RFAT agent, 4-cyano, 4-[(phenylcarbothioyl) sulfanyl] pentanoic acid, was synthesized in our laboratory [38]. The initiator 2, 2′-azobisisobutyronitrile (AIBN, Fluka, Switzerland) was recrystallized from ethanol at 50°C before use. Tetrahydrofuran (THF) and toluene (Merck, Darmstadt, Germany) were dried by refluxing over sodium and distilled under argon atmosphere before use. Styrene (St) and acrylic Acid (AA) monomers were dried by calcium hydride and sodium sulfate, respectively, and then, distilled under reduced pressure. Ferrous chloride tetrahydrate ($FeCl_2.4H_2O$, 99%), ferric chloride hexanhydrate ($FeCl_3.6H_2O$, 98%), and oleic acid were purchased from Merck and used as received. All other reagents were purchased from Merck or Sigma-Aldrich (St. Louis, MO, USA) and purified based on the standard methods.

2.2. Synthesis of the RAFT agent

2.2.1. Synthesis of 4-methoxy benzencarbodithioic acid

Magnesium turnings (1.0 g, 0.04 mol), a crystal of iodine as a catalyst, and dried THF (10 mL) were placed in a 250-mL four-neck flask, fitted with two dripping funnels containing (4.2 mL, 0.04 mol) 4-bromoanisole in one and dried THF (30 mL) in the other, a condenser, a thermometer, and a magnetic stirrer. A few drops of 4-bromoanisole were added from the dripping funnel into the flask. The content of the reaction flask was then heated gently, with stirring, until the reaction started. The reaction started when the yellow color of iodine disappeared and a clear white solution was formed. At this time, THF (500 μL) was dropped to the flask and then, the 4-bromoanisole residue was added dropwise from the dripping funnel. It should be pointed out that the reaction temperature was controlled at 35 to 40°C. When the reaction was complete, the Grignard reagent was gently neutralized by slowly adding cold water (250 mL) from a separate funnel into which the synthesized product had been poured. The solvent was removed using a rotary evaporator.

2.2.2. Synthesis of bis(4-methoxy diphenyl) dithioperoxy anhydride

The synthesized 4-methoxy benzencarbodithioic acid is an unstable compound; therefore, it was used directly after removal of the solvent from the reaction flasks. The preparation of bis(4-methoxy diphenyl) dithioperoxy anhydride was carried out by the reaction of dimethyl sulfoxide (DMSO) with 4-methoxybenzenecarbodithioic acid. For this purpose, a 250-mL round-bottom flask was charged with 4-methoxy benzenecarbodithioic acid (6.17 g, 0.04 mol), DMSO (6.25 g, 0.08 mol), a catalytic amount of iodine, and absolute ethanol (100 mL). The reaction mixture was stirred mechanically at room temperature for about 50 minutes. Afterwards, the reaction was terminated through hermetic sealing (using Parafilm) of the flask and placing it in a refrigerator overnight in order to speed up the crystallization. The appearance of pink crystals confirmed the completion of the reaction. The crystals were washed with cold ethanol (200 mL), filtered, and dried overnight (yield: 83%).

2.2.3. Synthesis of 4-cyano-4-[(phenylcarbothioyl) sulfanyl] pentatonic acid (CTA)

Bis(4-methoxy phenyl) dithio peroxy anhydride (3.37 g, 0.007 mol) and 4,4-azobis (4-cyanopentatonic acid) (3.37 g, 0.007 mol) were dissolved in ethyl acetate (100 mL). The solution was placed in a 250-mL two-neck flask fitted with a reflux condenser and a thermometer. The solution was heated overnight at 85°C while being purged with nitrogen. After removing the solvent using a rotary evaporator, the resulting product was subjected to column chromatography using a

mixture of n-hexane and ethyl acetate (1:2 v/v), to afford an oily red compound.

2.3. Synthesis of PSt-CTA macro-RAFT agent

The 4-cyano-4-[(phenylcarbothioyl) sulfanyl] pentatonic acid was used as the Chain Transfer Agent (CTA). A solution containing styrene monomer (16.5 mL), RAFT agent (0.5 g), AIBN initiator (0.08 g), and dried toluene (13 mL) as a solvent was placed into a 50-mL two-neck flask equipped with a condenser, gas inlet/outlet, a thermometer, and a magnetic stirrer. At first, the reaction mixture was de-aerated for some minutes using argon gas at 0°C and then, stirred for 16 hours in an oil bath at 70°C. After this period, the flask was immersed in cold water and the polymerization process was suppression. To collect the obtained PSt-CTA polymer (as a macro-RAFT agent), the content of the flask was added to cold methanol, as the anti-solvent, dropwise. The obtained sediment was filtered and dried in vacuum at room temperature.

2.4. Synthesis of PSt-b-PAA block copolymer via RAFT polymerization technique

A 50-mL three-neck flask was charged with purified acrylic acid monomer (1.0 mL), macro-RAFT agent (PSt-CTA; 0.3 g), and toluene (10 mL). The AIBN initiator (5.5 mg, 1 wt.% relative to the monomer) was added to the flask. The reaction mixture was de-aerated for 15 minutes using argon gas at 0°C and then, polymerization temperature was set to 70°C using an oil bath. Polymerization was allowed to proceed at the mentioned temperature for about 24 hours under argon atmosphere. After this period, the flask was immersed in cold water and the polymerization process was suppression. The PSt-b-PAA was precipitated by cold methanol and then, the product was dried at room temperature in vacuum oven.

2.5. Synthesis of the nanocomposite

2.5.1. Synthesis of Fe_3O_4 NPs

$FeCl_2.4H_2O$ (1.5 g) and $FeCl_3.6H_2O$ (4.7 g) were dissolved in HCl solution (20 mL, 0.4 $molL^{-1}$). An NaOH solution (200 mL, 1.5 $molL^{-1}$) and a magnetic stirrer were placed in a 250-mL two-neck flask, fitted with a dripping funnel and a gas scrubber. The dripping funnel was filled with iron chlorides solution, which had previously been prepared. After gas scrubbing of the system using argon, the solution in the dripping funnel was added into the reaction flask, dropwise, with quick stirring at room temperature. As soon as the drops entered the flask, black color appeared. Dropwise addition was continued at constant speed until the solution of dripping funnel was consumed completely. The reaction should be in oxygen-free environment. After completion of the reaction, the resultant product was centrifuged and washed with deionized water several times, and dried at 60°C in reduced pressure.

2.5.2. Modification of Fe_3O_4 NPs

In the first step, Fe_3O_4 NPs (2.0 g) were spread into a mixture of ethanol and water (20 mL, 1:1 v/v) at a constant speed. After decantation of the floating solution on the sediment, it was washed with ethanol three times and dried at 40°C for 10 hours. In the final step, by adding distilled water (40 mL) and oleic acid (1.3 g) and stirring for one hour, performing in line with the first step, oleic acid-modified Fe_3O_4 NPs were obtained.

2.5.3. Synthesis of PSt-b-PAA/magnetic nanocomposite

The PSt-b-PAA/Fe_3O_4 magnetic nanocomposite was obtained through solution mixing as follows. Fe_3O_4 NPs (0.5 g), PSt-b-PAA copolymer (2.0 g), and THF (10 mL) were placed in a round-bottom flask. Then, while stirring, distilled water (20 mL) was added to the reaction medium at a speed of 2 mL per minute. The filtering solids were washed thoroughly with petroleum ether and then, dried in vacuum for 24 hours to obtain PSt-b-PAA/Fe_3O_4 magnetic nanocomposite.

2.6. Characterization

Fourier transform infrared (FTIR) spectra of the samples were collected on a Shimadzu 8101M FTIR (Shimadzu, Kyoto, Japan) between the frequency ranges of 4000 to 400 cm^{-1} with attenuated total reflection facility. The samples were prepared by grinding the dry powders with potassium bromide (KBr) and compressing the mixture into disks. The spectra were recorded at room temperature. The proton nuclear magnetic resonance (^{1}H NMR) spectroscopy was carried out on Varian INOVA-500 (Palo Alto, CA, USA) using $CDCl_3$ as the solvent. The morphology and size distribution of the particles were obtained using a transmission electron microscope (TEM; CM10-TH microscope, Philips, Eindhoven, The Netherlands) and scanning electron microscope (SEM; type 1430 VP, LEO Electron Microscopy Ltd, Cambridge, UK). The thermogravimetric analysis (TGA) was carried out on a TGA/DSC apparatus (Pyris-1, Perkin-Elmer) with heating rate of 10°C/min in flowing high-purity nitrogen gas with 20 mL/min. Gel Permeation Chromatography (GPC) was performed with a Waters 150C detector. Measurements on GPC were performed in THF solvent at 45°C with 1.0 mL/min flow and calibration based on a set of mono disperse polystyrene standards. The X-Ray Diffraction (XRD) patterns were obtained with a Siemens D 5000 (Aubrey, Texas, USA) X-ray generator (CuKα radiation with λ = 1.5406 Å) with a 2θ scan range of 10 to 50° at room temperature.

3. Result and discussion

3.1. Characterization of the 4-cyano-4-[(phenylcarbothioyl) sulfanyl] pentatonic acid

RAFT polymerization achieves living growth starting from the initial dithioester or trithiocarbonate RAFT agent, which is activated by radicals generated from a traditional initiator. The synthesized RAFT agent was characterized using FTIR and ^{1}H NMR techniques. The FTIR spectrum of the bis(4-methoxydiphenyl) dithioperoxy anhydride (Figure 1(a)) exhibited characteristic absorption bands including S-S bending vibration at 560 cm^{-1}, the stretching vibration of C–S at 584 cm^{-1}, the stretching vibration of C=C at 1441 and 1593 cm^{-1}, and C–O stretching vibration at 1242 cm^{-1}.

In FTIR spectrum of 4-cyano-4-[(phenyl carbon thioyl) solfanyl pentatonic acid (Figure 1(b)), if the desired compound is synthesized correctly, the vibrations of the C–N, C=O, and –OH groups should be visible. By comparing Figure 1(a) and (b), three additional absorption peaks appear at 1600 cm^{-1} to 3600 cm^{-1}, which belong to C=O, C–N, and –OH, respectively. There is a small peak at 2300 cm^{-1}, which is related to stretching vibration of the C–N group. In addition, the broad band at 2600 cm^{-1} to 3600 cm^{-1} is related to the stretching vibration of acidic –OH. Also, the stretching vibration of C=O is seen at 1680 cm^{-1} and the absorption bands in 1441 and 1595 cm^{-1} are attributed to aromatic C=C bond of the RAFT agent.

Figure S1 (see Supplementary Information) shows the ^{1}H NMR spectrum of 4-cyano-4-[(phenyl carbon thioyl) sulfanyl pentatonic acid recorded in $CDCl_3$. The chemical shifts observed at 7-8 ppm are attributed to the aromatic hydrogens on the benzene ring. The resonances of about 1.0-2.0 and 4.0 ppm are related to the aliphatic protons of the sample. Overall, the obtained spectrum matches the reference spectrum, but there are some impurities.

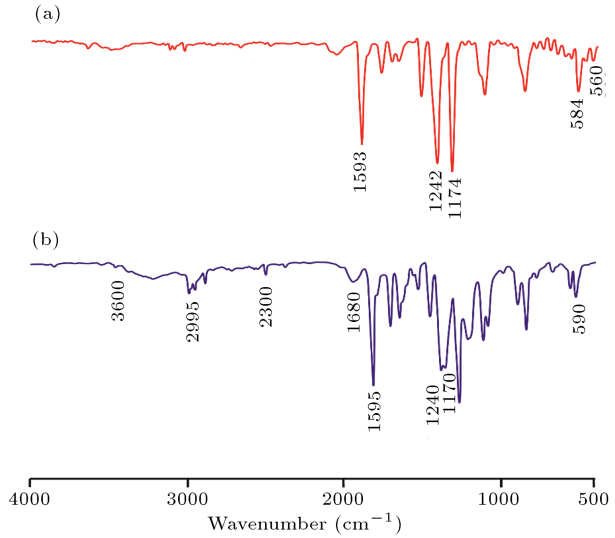

Figure 1. The FTIR spectra of (a) bis(4-methoxy diphenyl) dithioperoxy anhydride and (b) 4-cyano-4-[(phenylcarbonothioyl) sulfanyl] pentatonic acid.

3.2. Characterization of the PSt-CTA, PSt-b-PAA, and PSt-b-PAA/Fe_3O_4 magnetic nanocomposites

Figure 2 shows the FTIR spectra of PSt-CTA (a) and PSt-*b*-PAA (b). The most important absorption bands in the FTIR spectrum of the PSt-CTA can be named as the stretching vibration of the aromatic and aliphatic C–H at 3100-2800 cm^{-1} region, the stretching vibrations of C=C at 1598 and 1492 cm^{-1}, and γ(C–H) in the aromatic ring at 756 and 698 cm^{-1}. After block copolymerization of AA monomer onto PSt-CTA macro-initiator, the most significant changes are the appearance of C–O stretching vibration at 1193 cm^{-1}, the stretching vibration of carbonyl group at 1714 cm^{-1}, and the stretching vibration of hydroxyl group as a broad band centered at 3000 cm^{-1}.

The ^{1}H NMR spectroscopy was used to verify the chemical structures of the synthesized PSt-CTA macro-RAFT agent and PSt-*b*-PAA copolymer as shown in Figure S2 (see Supplementary Information). In ^{1}H NMR spectrum of the PSt-CTA (Figure S2(a) in Supplementary Information), the aromatic protons of PSt appear at 6.3-7.4 ppm. The aliphatic protons of methylene group (attached to SP^3 carbon) appear around 1.2-1.8 ppm and the proton of methyn group appears in a high area compared to the first and second hydrogens at 2.3 ppm. The ^{1}H NMR spectrum of the PSt-*b*-PAA (Figure S2(b) in Supplementary Information) shows the chemical shifts of PSt same as those observed in Figure S2(a). In addition, the methyn

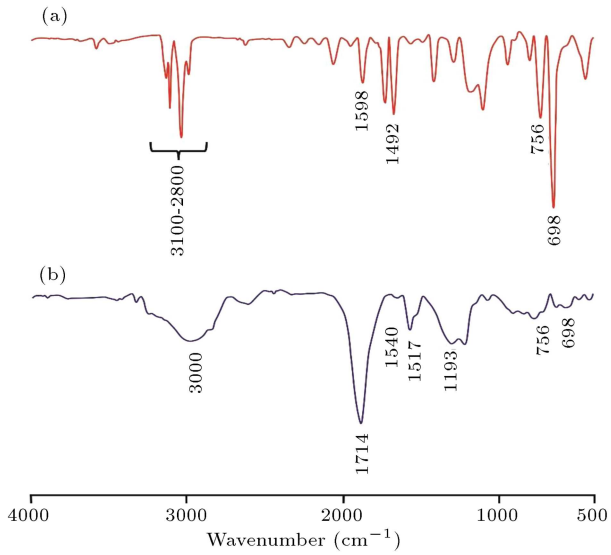

Figure 2. The FTIR spectra of (a) PSt-CTA and (b) P St-*b*-PAA.

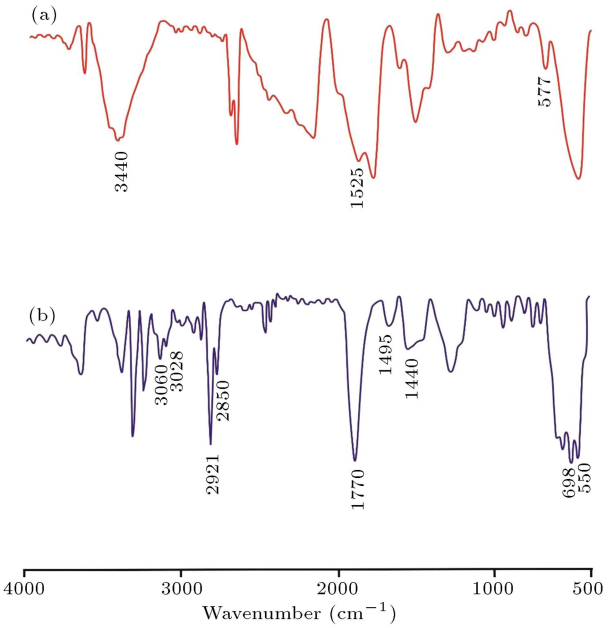

Figure 3. The FTIR spectra of (a) Fe_3O_4 NPs and (b) PSt-*b*-PAA/Fe_3O_4 magnetic nanocomposite.

protons of AA units are observed around 1.85 ppm. Based on the ^{1}H NMR spectra, it is confirmed that PSt-*b*-PAA is successfully synthesized, implying that the block copolymer contains PSt and PAA segments.

The FT-IR spectra of Fe_3O_4 NPs (a) and PSt-*b*-PAA/Fe_3O_4 magnetic nanocomposite (b) are shown in Figure 3. According to the FTIR spectrum of Fe_3O_4 NPs, the absorption band at 577 cm^{-1} belongs to the stretching vibration mode of Fe–O bonds in Fe_3O_4. The broad band at 3440 cm^{-1} is due to the stretching vibration of the –OH groups and the band at 1525 cm^{-1} is related to the hydroxyl bending vibration on the surface of Fe_3O_4 NPs (Figure 3(a)). For PSt-*b*-PAA/Fe_3O_4 magnetic nanocomposite, the absorption band at 550 cm^{-1} is the characteristic band of Fe–O, the bands at 1440 and 1495 cm^{-1} are the characteristic vibration absorption bands of C=C, the stretching vibration of aliphatic and aromatic C–H is at 3100-2850 cm^{-1}, and γ(C–H) in the aromatic rings is at 698 cm^{-1}. In addition, the absorption bands at 1440 and 1770 cm^{-1} belong to the bending vibrations of –CH and C=O groups in PAA segment. The characteristic absorption bands of St and AA as well as Fe_3O_4 are presented in Figure 3(b), which confirm the successful synthesis of PSt-*b*-PAA/Fe_3O_4 magnetic nanocomposite.

3.3. GPC analysis of PSt-CTA and PSt-b-PAA

The number-average molecular weight (M_n) and polydispersity index (PDI) of PSt-CTA macro-RAFT agent and PSt-*b*-PAA copolymer were measured using GPC as shown in Figure 4. The PDI of the synthesized

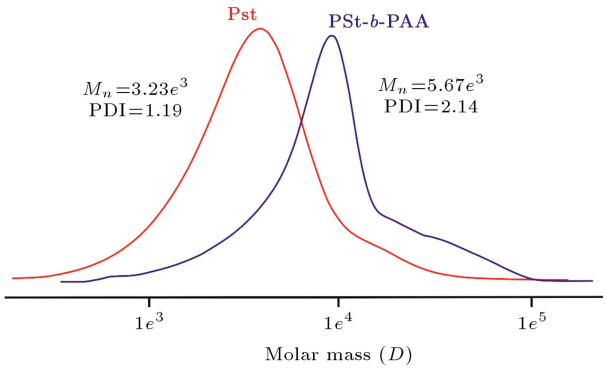

Figure 4. GPC chromatograms of PSt and PSt-*b*-PAA.

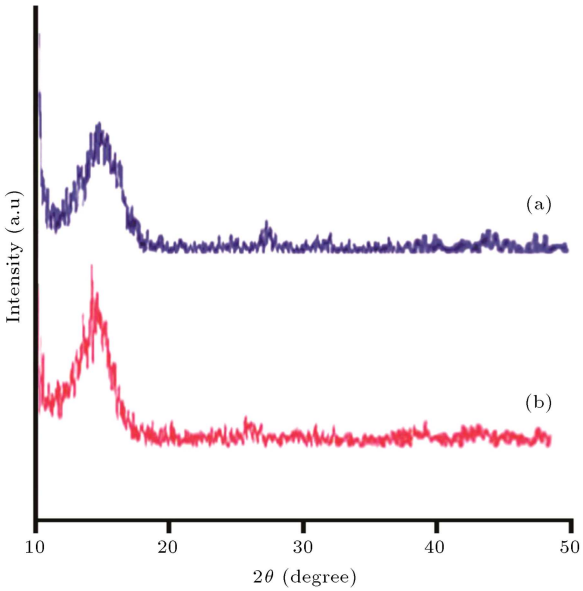

Figure 5. The XRD patterns of (a) Fe_3O_4 NPs and (b) PSt-*b*-PAA/Fe_3O_4 magnetic nanocomposite.

PSt was 1.19, indicating good control during the polymerization process. However, both M_n and PDI values increased after block copolymerization of AA monomer onto PSt-CTA macro-RAFT. In addition, the single GPC peaks for both samples suggested that there was no homopolymer contamination.

3.4. X-ray diffraction study

The crystalline structures of the Fe_3O_4 NPs and PSt-*b*-PAA/Fe_3O_4 magnetic nanocomposite were characterized using XRD as shown in Figure 5. It is apparent that the diffraction pattern of Fe_3O_4 NPs is close to the standard pattern for crystalline magnetite. The diffraction peaks at 2θ = 15.4, 18.5, 26.4, 43.2, and 48.0° can be well indexed to (220), (311), (400), (511), and (440) for Fe_3O_4 crystalline structure, respectively. The average crystalline size (D) of the synthesized Fe_3O_4 NPs was calculated to be 20 nm by the Debye-Scherrer formula [$D = k\lambda/(\beta\cos\theta)$] [39,40] (Figure 5(a)). As seen in Figure 5(b), the developed PSt-

b-PAA/Fe_3O_4 magnetic nanocomposite shows similar diffraction peaks to those of Fe_3O_4 NPs; however, the intensities of its diffraction peaks become significantly lower. This phenomenon may originate from the conjugation of the amorphous polymer (PSt-b-PAA) with crystalline Fe_3O_4 NPs.

3.5. Morphology study

The surface morphologies of the synthesized PSt-b-PAA and PSt-b-PAA/Fe_3O_4 magnetic nanocomposites were observed by means of SEM and TEM. The SEM image of the PSt-b-PAA exhibited compressed microstructure. The growth of PAA segments onto PSt-CTA, which was clearly seen in the SEM image, led to wrinkled morphology and some protuberances appeared on the surface, mainly due to immiscibility of PSt and PAA (Figure 6(a)).

In contrast, after self-assembly of the synthesized PSt-b-PAA onto the Fe_3O_4 NPs, the sizes of the particles decreased significantly. According to the SEM image, the average size of the PSt-b-PAA/Fe_3O_4 magnetic nanocomposite is estimated to be about 80 ± 30 nm. In addition, the synthesized PSt-b-PAA can be adsorbed onto the Fe_3O_4 NPs through the physical interactions between the carboxyl groups of PAA segment and surface hydroxyl groups of Fe_3O_4 NPs (Figure 6(b)).

TEM micrograph of the obtained PSt-b-PAA/Fe_3O_4 magnetic nanocomposite showed that Fe_3O_4 NPs were well dispersed in the polymeric matrix. However, agglomeration of Fe_3O_4 NPs could be observed in the sample. This excellent dispersion originated from the strong interaction (e.g., hydrogen bonding and ionic interactions) between the carboxyl groups of PAA segment and surface hydroxyl groups of Fe_3O_4 NPs, as mentioned above (Figure 6(c)).

3.6. Study of thermal properties

3.6.1. TGA study

TGA was used to investigate the thermal degradation occurring in the course of heating under nitrogen flow in PSt-CTA, PSt-b-PAA, and PSt-b-PAA/Fe_3O_4 magnetic nanocomposites as shown in Figure 7. As seen, no significant mass loss occurred until 300°C in PSt-CTA. Overall, only about 9 wt.% weight loss was observed in the initial sample weight, originating from the release of water and toluene solvent or small molecules (e.g., CTA). The main thermal decomposition, which started at 300°C and ended at 470°C with weight loss of 87 wt.%, resulted from the degradation of the polymer chains. Monomeric products along with significant amounts of oligomers and small amounts of benzene and toluene were produced. Total weight loss of PSt-CTA was 98.5 wt.%.

The TGA curve of PSt-b-PAA block copolymer exhibits three distinct zones of weight loss processes. The initial weight loss at 40 to 170°C is related to the traces of moisture and any organic solvent present in the sample or small molecules (6 wt.%). The second step of weight loss at 170 to 360°C (39 wt.%) is related to de-carboxylation and anhydride formation in the PAA segments [41]. The final weight loss at 360 to 450°C is associated with degradation of the PSt and poly(acrylic anhydride) backbones (37 wt.%), after which the loss rate slows down. The residue at 600°C for this sample is about 4 wt.%.

In contrast, the TGA curve of the obtained PSt-b-PAA/Fe_3O_4 magnetic nanocomposite exhibits two

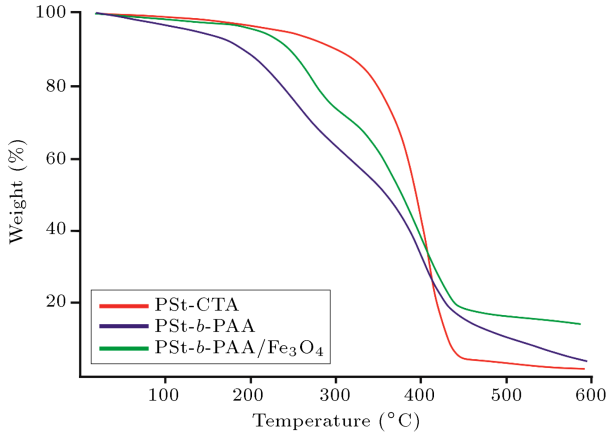

Figure 7. The TGA traces of the PSt-CTA, PSt-b-PAA, and PSt-b-PAA/Fe_3O_4 magnetic nanocomposites.

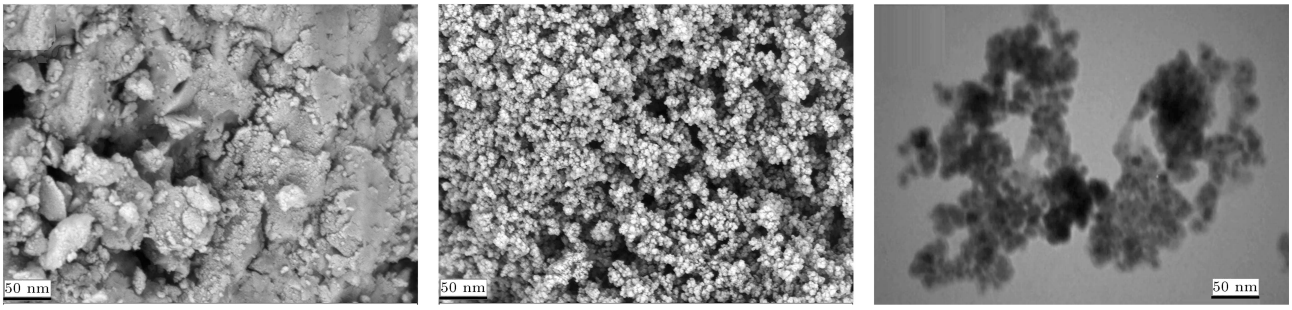

Figure 6. The SEM images of PSt-b-PAA (a) and SEM (b), and TEM image (c) of PSt-b-PAA/Fe_3O_4 magnetic nanocomposite.

main distinct zones for weight loss processes. The degradation starts with the release of adsorbed water at 50 to 200°C (∼4 wt.%). The first main stage, which starts at 200°C and ends at 310°C with weight loss of 23 wt.% results from de-carboxylation and anhydride formation in the PAA segments. It should be pointed out that the small molecules including oleic acid and CTA may degrade at this stage. The second main stage, which starts at 310°C and ends at 440°C with weight loss of 53 wt.%, is mainly attributed to the degradation of the PSt and poly(acrylic anhydride) backbones. The residue at 600°C for this sample is 17 wt.% of which the main portion is related to the higher stability of Fe_3O_4 NPs. Finally, as seen, the incorporation of Fe_3O_4 NPs into the PSt-*b*-PAA improves its thermal stability.

3.6.2. DSC study

The thermal behavior of PSt-CTA, PSt-*b*-PAA, and PSt-*b*-PAA/Fe_3O_4 magnetic nanocomposites was also investigated by means of DSC, as shown in Figure 8. As known, PSt is an amorphous thermoplastic; therefore, its physical state changes before reaching the melting temperature. The melting temperature (T_m) and glass transition temperature (T_g) of PSt at references are 240°C and 100°C, respectively. As shown in Figure 8(a), T_g and T_m of the PSt-CTA are 142 and 245°C, respectively. The peak at 65°C results from the evaporation of the solvent or moisture content of the polymer.

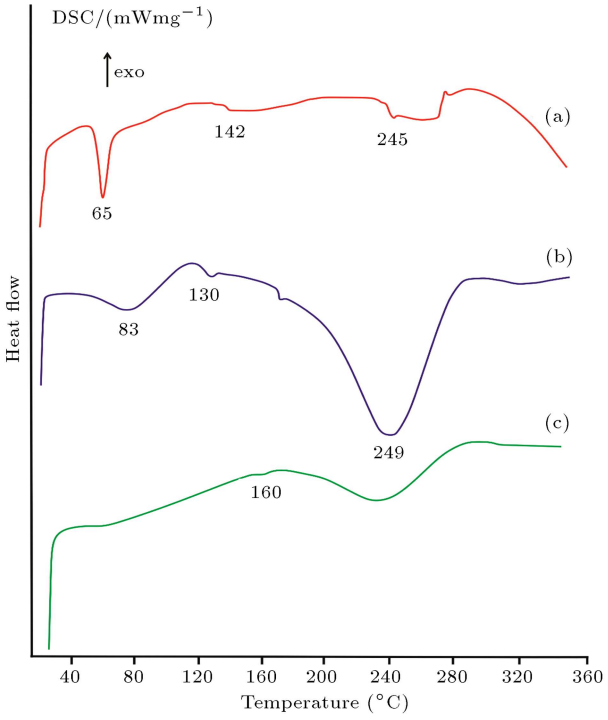

Figure 8. The DSC traces of the PSt-CTA (a), PSt-*b*-PAA (b), and PSt-*b*-PAA/Fe_3O_4 magnetic nanocomposites (c).

The DSC trace of PSt-*b*-PAA block copolymer (Figure 8(b)) has two main endothermic peaks at 83 and 249°C; the first one may be due to the evaporation of the solvent and the moisture content of the polymer, and the second one results from the intermolecular and intramolecular dehydration of PAA segment. T_g for this sample is 130°C, which increases due to impeding chain movement after block copolymerization of AA monomer onto PSt-CTA maroinitiator. T_g for the PSt-*b*-PAA/Fe_3O_4 magnetic nanocomposite (Figure 8(c)) is 160°C, which increases significantly due to strong interaction of polymeric chains (especially, PAA segment) with Fe_3O_4 NPs.

4. Conclusion

A well-defined PSt-*b*-PAA/Fe_3O_4 magnetics nanocomposite was synthesized using a versatile method through RAFT technique. The successful synthesis of PSt-*b*-PAA copolymer was verified using FTIR, ^{1}H NMR, and GPC analyses. The SEM and TEM images revealed that the synthesized PSt-*b*-PAA could be adsorbed onto Fe_3O_4 NPs toward the formation of nanocomposite in the size range of 80 ± 30 nm. According to the TEM image, Fe_3O_4 NPs were well dispersed in the PSt-*b*-PAA matrix, mainly due to strong interactions between the carboxyl groups of PAA segment and surface hydroxyl groups of Fe_3O_4 NPs. The successful synthesis of the above-mentioned materials was also verified through TGA and DSC analyses. It was fund that the incorporation of Fe_3O_4 NPs into PSt-*b*-PAA copolymer increased its T_g value as well as thermal stability. The developed PSt-*b*-PAA/Fe_3O_4 magnetic nanocomposite may be applied for enzyme immobilization and cell separation.

Supplementary information

Supplementary Information is available at:
http://scientiairanica.sharif.edu/jufile?ar_sfile=114452

Acknowledgement

The authors thank Payame Noor University for supporting this project.

References

1. Hassanzadeh, Sh., Eisavi, R., Abbasian, M. "Preparation and characterization of magnetically separable $MgFe_2O_4/Mg(OH)_2$ nanocomposite as an efficient heterogeneous catalyst for regioselective one-pot synthesis of β-chloroacetates from epoxides", *Applied Organometallic Chemistry*, **32**, e4520 (2018).
2. Laurent, S., Forge, D., Port, M., Roch, A., and Robic, C.L. "Preparation of poly(styrene)-

b-poly(acrylicacid)/γ-Fe_2O_3 composites", *J. Magn. Magn. Mater.*, **323**, pp. 3087-3091 (2011).

3. Laurent, S., Forge, D., Port, M., Roch, A., Robic, C.L., Vander, E., and Muller, R. "Preparation and drug-loading properties of Fe_3O_4/poly(styrene-co-acrylic acid) magnetic polymer nanocomposites", *J. Magn. Magn. Mater.*, **345**, pp. 142-146 (2013).

4. Jiang, J., Gan, Z., Yang, Y., Du, B., Qian, M., and Zhang, P.J. "Preparation of magnetic poly (styrene-co-acrylic acid) microspheres with adsorption of protein", *Colloid. Surface A.*, **443**, pp. 425-431 (2014).

5. Xie, G., Zhang, Luo, Q.Z., Wu, M., and Li, T. "Preparation and characterization of monodisperse magnetic poly(styrene butyl acrylate methacrylic acid) microspheres in the presence of a polar solvent", *J. Appl. Polym. Sci.*, **87**, pp. 1733-1738 (2003).

6. Philippova, O., Barabanova, A., Molchanov, V., and Khokhlov, A. "Magnetic polymer beads: Recent trends and developments in synthetic design and applications", *Eur. Polym. J.*, **47**, pp. 542-559 (2011).

7. Luong, T.T., Ha, T.P., Tran, L.D., Do, M.H., Mai, T.T., Pham, N.H., Phan, H.B.T., Pham, G.H.T., My, N., Quy, T.H., Phuc T.N., and Nguyen, X. "Design of carboxylated Fe_3O_4/poly(styrene-co-acrylic acid) ferrofluids with highly efficient magnetic heating effect", *Colloid. Surface A.*, **384**, pp. 23-30 (2011).

8. Ahmadkhani, L., Akbarzadeh, A., and Abbasian, M. "Development and characterization dual responsive magnetic nanocomposites for targeted drug delivery systems", *Artificial Cells, Nanomedicine, and Biotechnology*, **46**(5), pp. 1052-1063 (2018).

9. Li, R., Fu, G., Liu, C., McClements, D.J., Wan, Y., Wang, S., and Liu, T. "Tannase immobilisation by amino-functionalised magnetic Fe_3O_4-chitosan nanoparticles and its application in tea infusion", *Int. J. Biol. Macromol.*, **114**, pp. 1134-1143 (2018).

10. Hayasi, M. and Karimi, M. "Synthesis of poly(styrene-co-methacrylic acid)-coated magnetite nanoparticles as effective adsorbents for the removal of crystal violet and Rhodamine B: a comparative study", *Polym. Bull.*, **74**, pp. 1995-2016 (2017).

11. Pimpha, N., Chaleawlertumpon, S., Chruewkamlow, N., and Kasinrerk, W. "Preparation of anti-CD_4 monoclonal antibody-conjugated magnetic poly (glycidylmethacrylate) particles and their application on CD_4+lymphocyte separation", *Talanta*, **84**, pp. 89-97 (2011).

12. Xiong, B., Wang, N., Chen, Y., and Peng, H. "Self-assembly of alginate/polyethyleneimine multilayer onto magnetic microspheres as an effective adsorbent for removal of anionic dyes", *J. Appl. Polym. Sci.*, **135**, p. 45876 (2018).

13. Wang, C., Wang, Y., Ouyang, Z., Shen, T., and Wang, X. "Preparation and characterization of polymer-coated Fe_3O_4 magnetic flocculant", *Sep. Sci. Technol.*, **53**, pp. 814-822 (2018).

14. Ilia, R., Liatsou, I., Savva, I., Vasile, E., Vekas, L., Marinica, O., Mpekris, F., Pashalidis, I., and Krasia-Christoforou, T. "Magnetoresponsive polymer networks as adsorbents for the removal of U(VI) ions from aqueous media", *Eur. Polym. J.*, **97**, pp. 138-146 (2017).

15. Hu, D., Wan, X., Li, X., Liu, J., and Zhou, C. "Synthesis of water-dispersible poly-L-lysine-functionalized magnetic Fe_3O_4-(GO-MWCNTs) nanocomposite hybrid with a large surface area for high-efficiency removal of tartrazine and Pb(II)", *Int. J. Biol. Macromol.*, **105**, pp. 1611-1621 (2017).

16. Wei, S., Zhang, Y., and Xu, J. "Preparation and properties of poly (acrylic acid-co-styrene) /Fe_3O_4 nanocomposites", *J. Polym. Res.*, **18**, pp. 125-130 (2011).

17. Burguière, C., Chassenieux, C., and Charleux, B. "Characterization of aqueous micellar solutions of amphiphilic block copolymers of poly (acrylic acid) and polystyrene prepared via ATRP", *Polymer.*, **44**, pp. 509-518 (2003).

18. Zhang, W.Q., Shi, L.Q., Miao, Z.J., Wu, K., and An, Y.L. "Core-shell corona micellar complexes between poly(ethylene glycol)-block poly(4-vinyl pyridine) and polystyrene-block-poly(acrylic acid)", *Macromol. Chem. Phys.*, **206**, pp. 2354-2361 (2005).

19. Guo, F.X., Jankova, K., Schulte, L., Vigild, M.E., and Ndoni, S. "One step routes from di- and triblock copolymer precursors to hydrophilic nanoporous poly(acrylic acid)-b-polystyrene", *Macromolecules.*, **41**, pp. 1486-1496 (2008).

20. Liu, G., Hong, R.Y., Guo, L., Li, Y.G., and Li, H.Z. "Preparation, characterization and MRI application of carboxymethyl dextran coated magnetic nanoparticles", *Appl. Surface. Sci.*, **257**, pp. 6711-6717 (2011).

21. Veiseh, O., Gunn, J.W., and Zhang, M.Q. "Design and fabrication of magnetic nanoparticles for targeted drug delivery and imaging", *Adv. Drug Deliver. Rev.*, **62**, pp. 284-304 (2010).

22. Xue, Y.N., Huang, Z.Z., Zhang, J.T., Liu, M., Zhang, M., Huang, S.W., and Zhuo, R.X. "Synthesis and self-assembly of amphiphilic poly (acrylic acid-b-DL-lactide) to form micelles for pH-responsive drug delivery", *Polymer*, **50**, pp. 3706-3713 (2009).

23. Li, G.H. and Cho, C.G. "CMC and dynamic properties of poly (VA-b-St) copolymer micelles for drug delivery", *Korean. J .Chem. Eng.*, **25**, pp. 1444-1447 (2008).

24. Oh, J.K. and Park, J.M. "Iron oxide-based superparamagnetic polymeric nanoma- terials: design, preparation, and biomedical application", *Prog. Polym. Sci.*, **36**, pp. 168-189 (2011).

25. Hautekeer, J.P., Varshney, S.K., Fayt, R., Jacobs, C., Jérôme, R., and Teyssié, P. "Anionic polymerization of acrylic monomers. 5. Synthesis, characterization, and modification of polystyrene-poly (tert-butyl acrylate) di- and triblock copolymers", *Macromolecules*, **23**, pp. 3893-3898 (1990).

26. Zhang, L.F. and Eisenberg, A. "Multiple morphologies and characteristics of "crew-cut" micelle-like aggregates of polystyrene-b-poly (acrylic acid) diblock copolymers in aqueous solutions", *J. Am. Chem. Soc.*, **118**, pp. 3168-3181 (1996).

27. Couvreur, L., Charleux, B., Guerret, O., and Magnet, S. "Amphiphilic gradient poly (styrene-co-acrylic acid) copolymer prepared via nitroxide-mediated solution polymerization. Synthesis, characterization in aqueous solution and evaluation as emulsion polymerization stabilizer", *Macromol. Chem. Phys.*, **47**, pp. 1935-1945 (2006).

28. Ghasemi Karaj-abad, S., Abbasian, M., and Jaymand, M. "Grafting of poly [(methyl methacrylate)-block-styrene] onto cellulose via nitroxide-mediated polymerization, and its polymer/clay nanocomposite", *Carbohyd. Polym.*, **152**, pp. 297-305 (2016).

29. Perrier, S. "50th anniversary perspective: RAFT polymerization - A user guide", *Macromolecules*, **50**, pp. 7433-7447 (2017).

30. Abbasian, M. and Mahi, R. "In-situ synthesis of polymer-silica nanocomposites by living radical polymerisation using TEMPO initiator", *J. Exp. Nanosci.*, **9**, pp. 785-798 (2014).

31. Mohammad-Rezaei, R., Massoumi, B., Abbasian, M., and Jaymand, M. "Novel strategies for the synthesis of hydroxylated and carboxylated polystyrenes", *J. Polym. Res.*, **25**, p. 93 (2018).

32. Mahmoodzadeh, F., Abbasian, M., Jaymand, M., and Amirshaghaghi, A. "A novel dual stimuli-responsive thiol-endcapped ABC triblock copolymer: synthesis via reversible addition-fragmentation chain transfer technique, and investigation of its self-assembly behavior", *Polym. Int.*, **66**, pp. 1651-1661 (2017).

33. Abbasian, M. and Khakpour, A.N. "Synthesis of poly (methyl methacrylate)/zinc oxide nanocomposite with core-shell morphology by atom transfer radical polymerization", *J. Macromol. Sci.*, **50**, pp. 966-975 (2013).

34. Abbasian, M., Shahparian, M., and Esmaeily Shoja, S. "Well-defined poly (methyl methacrylate) grafted to isotactic polypropylene by metal catalyzed living radical polymerization", *J. Elastom. Plast.*, **45**, pp. 317-331 (2013).

35. Abbasian, M. and Ahmadkhani, L. "Synthesis of conductive PSt-g-PANi/TiO_2 nanocomposites by metal catalyzed and chemical oxidative polymerization", *Desig. Monomers. Polym.*, **19**, pp. 585-595 (2016).

36. Abbasian, M., Massomi, B., Rashidzadeha, B., and Bahramia, H. "Versatile method for synthesis of electrically conductive polypyrrolepolystyrene clay nanocomposites using ATRP and chemical polymerisation methods", *J. Exp. Nanosci.*, **10**, pp. 844-858 (2015).

37. Abbasian, M., Ghaeminia, H., and Jaymand, M. "A facile and efficient strategy for the functionalization of multiple-walled carbon nanotubes using well-defined polypropylene-grafted polystyrene", *Appl. Phys A.*, **124**, p. 522 (2018).

38. Massoumi, B., Ghandomi, F., Abbasian, M., Eskandani, M., and Jaymand, M. "Surface functionalization of graphene oxide with poly(2-hydroxyethyl methacrylate)-graft-poly(ε-caprolactone) and its electrospun nanofibers with gelatin", *Appl. Phys A.*, **122**, p. 1000 (2016).

39. Mozaffari, Z., Hatamzadeh, M., Massoumi, B., and Jaymand, M. "Synthesis and characterization of a novel stimuli-responsive magnetite nanohydrogel based on poly(ethylene glycol) and poly(N-isopropylacrylamide) as drug carrier", *J. Appl. Polym. Sci.*, **135**, p. 46657 (2018).

40. Farnoudian-Habibi, A., Kangari, S., Massoumi B., and Jaymand, M. "Determination of Losartan potassium in the presence of hydrochlorothiazide via a combination of magnetic solid phase extraction and fluorometry techniques in urine samples", *RSC. Adv.*, **5**, pp. 102895-102903 (2015).

41. Mozaffari, Z., Massoumi, B., and Jaymand, M. "A novel stimuli-responsive magnetite nanocomposite as de novo drug delivery system", *Polym. Plast. Technol. Eng.*, **58**, pp. 405-418 (2019).

Biographies

Mojtaba Abbasian is Associate Professor in the Department of Chemistry at Payame Noor University, Tabriz, Iran. He received BS degree in Pure Chemistry in 2000, and MS and PhD degrees in Organic Chemistry (Polymer Science) in 2002 and 2007, respectively, all from University of Tabriz, Iran. His research interests include living radical polymerization, nanocomposite polymers, and drug delivery system.

Leyla Razavi received BS degree in Pure Chemistry and MS degree in Organic Chemistry (Polymer Science) from Payame Noor University, Tabriz, Iran, in 2012 and 2014, respectively. Her research interests include living radical polymerization, nanocomposite polymers, and drug delivery system.

Mehdi Jaymand is Assistant Possessor at Kermanshah University of Medical Sciences, Kermanshah,

Iran. He received BS degree in Pure Chemistry and MS degree in Organic Chemistry (Polymer Science) from Payame Noor University in 2007 and 2009, respectively, and PhD degree in Pharmaceutical Biotechnology from Tabriz University of Medical Sciences in 2117. His research interests include polymer chemistry and physics, tissue engineering, and drug delivery system.

Saber Ghasemi Karaj-Abad received BS degree in Pure Chemistry and MS degree in Organic Chemistry (Polymer Science) from Payame Noor University, Tabriz, Iran, in 2014 and 2016, respectively. His research interests include living radical polymerization, nanocomposite polymers, and drug delivery system.